

Thermal origin of quasi-localised excitations in glasses

Wencheng Ji¹, Tom W.J. de Geus¹, Marko Popović¹, Elisabeth Agoritsas¹, Matthieu Wyart¹

¹*Institute of Physics, École Polytechnique Fédérale de Lausanne (EPFL), CH-1015 Lausanne, Switzerland*

Abstract

Key aspects of glasses are controlled by the presence of excitations in which a group of particles can rearrange. Surprisingly, recent observations indicate that their density is dramatically reduced and their size decreases as the temperature of the supercooled liquid is lowered. Some theories predict these excitations to cause a gap in the spectrum of quasi-localised modes of the Hessian that grows upon cooling, while others predict a pseudo-gap $D_L(\omega) \sim \omega^\alpha$. To unify these views and observations, we generate glassy configurations of controlled gap magnitude ω_c at temperature $T = 0$, using so-called ‘breathing’ particles, and study how such gapped states respond to thermal fluctuations. We find that (i) the gap always fills up at finite T with $D_L(\omega) \approx A_4(T)\omega^4$ and $A_4 \sim \exp(-E_a/T)$ at low T , (ii) E_a rapidly grows with ω_c , in reasonable agreement with a simple scaling prediction $E_a \sim \omega_c^4$ and (iii) at larger ω_c excitations involve fewer particles, as we rationalise, and eventually become string-like. We propose an interpretation of mean-field theories of the glass transition, in which the modes beyond the gap act as an excitation reservoir, from which a pseudo-gap distribution is populated with its magnitude rapidly decreasing at lower T . We discuss how this picture unifies the rarefaction as well as the decreasing size of excitations upon cooling, together with a string-like relaxation occurring near the glass transition.

1 Introduction

A key feature of structural glasses is that groups of particles can rearrange locally between two metastable states. This motion can be triggered by quantum or thermal fluctuations, or mechanically by exerting an external stress or strain. Such rearrangements are associated with different excitations. At low temperature the dominant source of excitations are two-level systems (TLS) that stem from quantum tunnelling between the metastable states [1–3]. At higher temperatures, relaxation in supercooled liquids near the glass transition occurs via thermally activated events, observed to become more and more string-like upon cooling [4, 5]. Upon mechanical loading, at any temperature below the glass transition, plasticity occurs when a group of particles becomes unstable. In the potential energy landscape, this corresponds to a saddle-node bifurcation [6, 7] and leads to a rearrangement denoted ‘shear transformation’ [8]. Understanding how temperature or system preparation controls the density of these excitations remains a challenge. It is, however, a question of practical importance since: (i) the density of shear transformations controls for instance the glass brittleness [9–11], (ii) the rarefaction of activated events near the glass transition controls its fragility [12], and (iii) the density of TLS (recently observed to be almost absent

in ultra-stable glasses [13, 14]) affects the decoherence in qubits [15] important for quantum computing. Finally, the possible unification of these excitations into a common description is a fundamental problem for a prospective theory of glasses.

These localised excitations should affect the low-frequency spectrum of the Hessian of the energy landscape, since groups of particles that can easily rearrange tend to have a small linear restoring force [6, 16, 17]. Indeed, in numerical glasses, such quasi-localised modes are found at low-frequencies [18]. Recently there has been a considerable effort to analyse them [19–25]. In most glasses, it is found that in inherent structures¹, the density of quasi-localised modes $D_L(\omega) \approx A_4(T)\omega^4$, with ω the frequency. Most remarkably, $A_4(T)$ is reduced by several decades as T is reduced by 30% [25, 26] (a similar finding was obtained for the density of TLS [27]). Furthermore, quasi-localised modes also display a lower participation ratio at lower T . A unifying explanation for these facts is currently missing². On the the-

¹Obtained by rapidly quenching an equilibrated liquid (at initial temperature T) to zero temperature.

²TLS were proposed to be controlled by the so-called mosaic length scale that diverges at the Kauzmann temperature T_K in mean field approaches [28]. Yet this description predicts a growing (instead of decreasing) length scale and a mild (a factor 10 at most) decrease of density of excitations upon cooling.

oretical side, two distinct approaches have been proposed. On the one hand, the ω^4 power law has been rationalised by making specific assumptions on the disorder and by assuming modes as non-interacting [29, 30], or by modelling a quench from $T = \infty$ and including interactions [17]. On the other hand, in mean-field calculations in infinite dimensions for temperatures below the mode-coupling temperature T_c [31] the spectrum of the Hessian becomes gapped (excluding obvious long wave-length Goldstone modes that are always present). Below T_c , the gap is predicted to grow as T decreases [32–34]. A gap was also predicted from real-space stability arguments in finite dimensions for continuously polydisperse particles, at very low energies and zero temperature [35]. Nevertheless, it is currently unclear if a gap truly exists in finite dimension and at finite temperature.

In this article we seek a unifying scenario for these facts and different approaches, by studying the stability of gapped spectra with respect to thermal fluctuations. Specifically, we use ‘breathing’ particles³ [37] in order to generate athermal ultra-stable glasses of controlled gap magnitude ω_c . Then, as sketched in Fig. 1, we transiently reheat these glasses, with a standard molecular dynamics simulation, at a low temperature T_a for a duration t_a , before quenching them back to zero temperature. Our central results are that (a) thermal fluctuations, even small, destroy the gap and we recover a density $D_L(\omega) \approx A_4 \omega^4$; the prefactor $A_4(T_a, t_a)$ depends very mildly on t_a but presents an Arrhenius dependence on temperature with $A_4 \sim \exp(-E_a/T_a)$ (in our temperature units the Boltzmann constant $k_B = 1$). (b) The activation energy E_a rapidly increases with the gap magnitude ω_c . (c) We introduce a novel algorithm to decompose the rearrangements into elementary excitations, and find that they involve fewer particles for larger gap values, and eventually become string-like for our largest gap. We propose a scaling argument for their decreasing size. Overall, these results suggest to describe equilibrated liquids perturbatively as *gapped states decorated by thermally activated excitations whose characteristic energy is controlled by the gap itself*, leading to a contribution with $A_4 \sim \exp(-E_a(\omega_c(T))/T)$. We discuss the implications of this picture, sketched in Fig. 1, for the density of these various excitations, for their effect on plasticity and on low-temperature properties of glasses as well as for the glass transition.

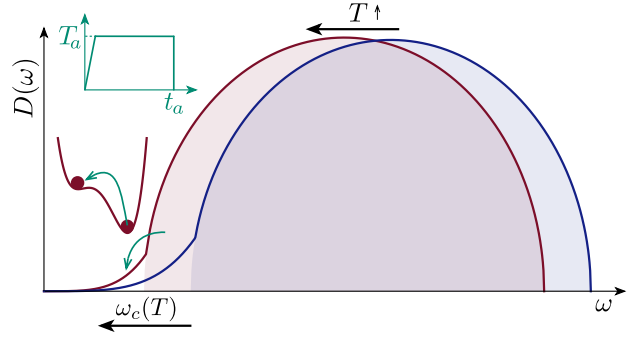


Figure 1. Schematic density of states for an equilibrated liquid at temperature T . When a gapped glass is heated to a temperature T_a for a duration t_a , as sketched in the inset, modes beyond the gap act as a reservoir of excitations that can be thermally activated. It fills up the gap, leading, for small ω , to a pseudo-gap $D(\omega) \approx D_L(\omega) \approx A_4 \omega^4$. This effect is exponentially diminished if ω_c increases (corresponding to a decrease of T as predicted by the infinite-dimensional mean-field description near the glass transition).

2 Generating gapped glasses

To generate ultra-stable glasses displaying a finite gap, we follow a procedure similar to [35]. We consider ‘breathing’ particles whose individual size can vary according to an energetic cost of characteristic stiffness K (see Appendix B). The particles interact with a repulsive potential, up to a finite cutoff radius, chosen such that the potential remains continuous up to its third derivative [38] and thus allowing for a well-defined Hessian. At a given temperature, this system is known to be thermodynamically equivalent to a system of given (and continuous) polydispersity, and can be simulated using a usual molecular dynamics (MD). Including this breathing degrees of freedom leads to a giant shortening of the equilibration time, comparable to that of swap algorithms [37, 39]. In practice, we perform MD with breathing particles for a long duration t_p at a temperature $T_p(K)$, chosen such as to minimise the energy of the states eventually obtained (see Appendix C), before quenching using a ‘FIRE’ algorithm [40] in which particles can still breathe.

The polydispersity obtained for various values of stiffness K is shown in Fig. 2(a) for $N = 8000$ particles, in three dimensions and at fixed pressure. Next, we freeze the radius of each particle, and compute the usual Hessian of the potential energy: its eigenvectors correspond to the vibrational modes of the glass, and its eigenvalues are denoted ω^2 since they correspond

³‘Breathing’ particles is an alternative version of swap algorithms in which particles of different radii are exchanged [36].

directly to the frequencies of vibrational modes, as we take the particle mass to be unity. Showing that these states are gapped requires considerable statistics; in fact, we collect the spectra of $n = 4000$ independent realisations (see Appendix A for a precise statement) and average them in order to obtain the density of vibrational modes $D(\omega)$. We emphasise that for the considered small system size, quasi-localised modes are already found below the first plane waves [20].

$D(\omega)$ turns out to display a gap: there are no quasi-localised modes below a finite frequency ω_c . Since we find ω_c to be even higher than the frequencies of the first plane waves for $K = \{10^2, 10^3\}$ we manually remove them in order to measure the density of *quasi-localised* modes $D_L(\omega)$, as shown in Fig. 2(b). We extract ω_c by fitting a power law $D_L(\omega) \sim (\omega - \omega_c)^\zeta$, and obtain the values $\omega_c = \{1.64, 1.19, 0.85, 0.65\}$, for $K = \{10^2, 10^3, 3 \times 10^3, 10^4\}$, indicated with markers in Fig. 2(b). Note that if we consider instead the minimal frequency observed as an estimate for ω_c , our conclusions below are not affected (see Appendix D).

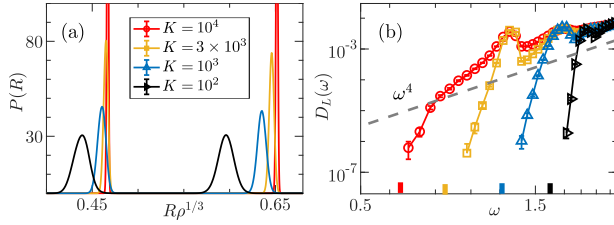


Figure 2. (a) Distribution of particle radii, normalised by the number density $\rho = N/\langle V \rangle$, for different values of stiffness K (the particle sizes are narrowly distributed when K is large). (b) Density of quasi-localised modes displaying a finite gap ω_c , in contrast to the usual pseudo-gap scaling $D_L(\omega) \sim \omega^4$ indicated with a dashed line. The gap values $\omega_c \approx \{1.64, 1.19, 0.85, 0.65\}$ corresponding respectively to $K = \{10^2, 10^3, 3 \times 10^3, 10^4\}$ are indicated using ticks, following the same color code. Physically, decreasing K results to a larger gap and thus a more stable glass, and is associated to a larger polydispersity.

3 Filling up the gap via thermal activation

To test the robustness of gapped states to thermal fluctuations, we reheat our samples to a temperature T_a and run MD simulations for a duration t_a , before applying an instantaneous quench to zero temperature. This procedure is sketched in Fig. 1 (and further detailed in Appendix B), and is entirely per-

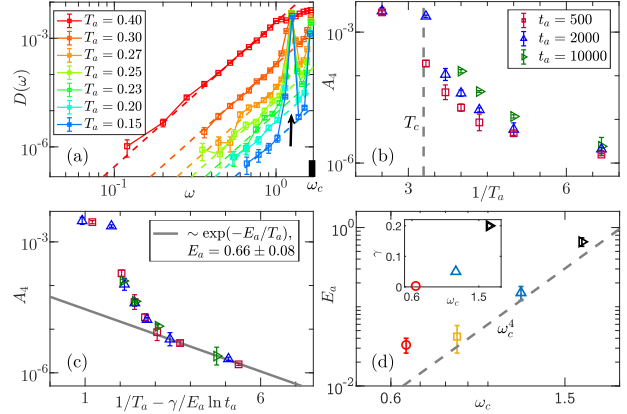


Figure 3. (a) Density of soft modes $D(\omega)$ after reheating for a fixed duration $t_a = 500$ at different temperatures T_a (following the protocol sketched in Fig. 1), at fixed gap $\omega_c = 1.64$ (the largest we generate, cf. Fig. 2). Note that the order of the legend matches the order of the curves. Furthermore, note that $D_L(\omega) = D(\omega)$ for $\omega < \omega_e$, with ω_e the frequency of the first plane wave, indicated with a black arrow. For reference, the mode-coupling temperature in this system is $T_c \approx 0.3$, and the gap, $\omega_c = 1.64$, is indicated by a black tick. We emphasise that, before reheating, we had $D_L(\omega < \omega_c) = 0$, so that the corresponding modes have been activated by thermal fluctuations. (b) Prefactor A_4 as a function of reheating temperature T_a for different durations t_a . (c) Collapse of the different curves $A_4(T_a, t_a)$, supporting the functional form $A_4 = f(t_a^\gamma \exp(-E_a/T_a))$ where the function f is linear at small argument, indicating an Arrhenius behaviour at small T_a . (d) Typical energy scale E_a vs the initial gap ω_c , together with the associated scaling prediction $E_a \sim \omega_c^4$ (dashed line). *Inset:* Dynamical exponent γ as a function of ω_c .

formed at fixed particle radii. Upon reheating, local rearrangements⁴ are thermally triggered (though less than 50% of the samples do rearrange at the lowest temperature that we probe⁵), consequently modifying the spectrum.

In Fig. 3(a) the low-frequency tail of $D(\omega)$ is shown for our stablest system (with $\omega_c = 1.64$) for $t_a = 500$ and varying T_a . Note that the acquisition of sufficient statistics required about 10^5 CPU hours. We always find that the gap is replaced by a pseudo-

⁴We define a rearrangement by a finite norm of the displacement field that results from reheating, see Appendix A for details.

⁵For our system size, at $t_a = 500$ (the time scale we use later), the temperature for which we have in average one rearrangement per realisation $T_a^*(\omega_c = 1.64) \approx 0.17$, which we estimate using the fit of the Arrhenius-like behaviour below.

gap, compatible with the standard scaling:

$$D_L(\omega) \approx A_4(T_a, t_a) \omega^4. \quad (1)$$

The prefactor A_4 characterises the density of quasi-localised excitations, and is extracted by fitting Eq. (1) for $\omega < \omega_e$, where ω_e is the frequency of the first plane wave (see Fig. 2(b)). As shown in Fig. 3(b), A_4 varies immensely (by three orders of magnitude), mostly due to the variation of the temperature T_a , with only a mild dependence on the time t_a . Moreover, we show in Fig. 3(c) that these curves can be collapsed, in the range of parameters probed, assuming the functional form $A_4(T_a, t_a) = f(t_a^\gamma \exp(-E_a/T_a))$ and $\gamma = 0.2$. The function f is linear at small argument, supporting an Arrhenius behaviour at low temperature T_a (see Appendix D). Remarkably, this collapse indicates that for a given gap, the distribution of excitation energies is characterised by a single energy scale E_a (presumably a lower cutoff, see below).

Interestingly, we find in Fig. 3(d) that E_a very strongly increases with gap magnitude ω_c (see below for a proposed explanation). The dynamical exponent $\gamma(\omega_c)$ is also shown in inset, and remains smaller than 0.2 in the entire range of initial gaps that we probe.

4 Modes beyond the gap act as an excitation reservoir

We saw that, if we start from a glass with an initially gapped density of states, thermal fluctuations will always populate this gap. To rationalise these findings, we consider the path of minimal energy connecting two states associated to one excitation, and denote by s the curvilinear coordinate along it. The Taylor expansion of the energy along this path from the state 1, by definition the one of minimal energy, reads:

$$E(s) = \frac{1}{2!} \lambda_1 s^2 + \frac{1}{3!} \kappa_1 s^3 + \frac{1}{4!} \chi_1 s^4 + \mathcal{O}(s^5) \quad (2)$$

which is a double-well, with a curvature $\lambda_1 \approx \omega_1^2$ around the minima in state 1. Physically, $\chi_1 > 0$ (otherwise the potential has no lower energy limit).

In that formalism, starting from a gapped glass corresponds to having a distribution $P(\lambda_1, \kappa_1, \chi_1)$ strictly zero at $\lambda_1 < \omega_c^2$ and smooth above ω_c^2 . At finite temperature the gap is populated by thermal activation towards a state 2 with a smaller frequency $\omega_2 \approx \sqrt{\lambda_2}$, which corresponds to a transition in an asymmetric double-well (as illustrated in Fig. 1). From Eq. (2) it is straightforward to obtain the

expansion from state 2, and the transformation $(\lambda_2, \kappa_2, \chi_2) = g(\lambda_1, \kappa_1, \chi_1)$. The joint distribution follows $P(\lambda_2, \kappa_2, \chi_2) = |g'(\lambda_2, \kappa_2, \chi_2)| P(\lambda_1, \kappa_1, \chi_1)$ where the absolute value of the determinant of the Jacobian $|g'(\lambda_2, \kappa_2, \chi_2)| \sim \lambda_2$ for small λ_2 (see Appendix E). Owing to the smoothness of $P(\lambda_1, \kappa_1, \chi_1)$ for $\lambda_1 \gtrsim \omega_c^2$, for small λ_2 one has $P(\lambda_2, \kappa_2, \chi_2) \sim \lambda_2$ or equivalently $P(\omega_2, \kappa_2, \chi_2) \sim \lambda_2 d\lambda_2/d\omega \sim \omega_2^3$. After integrating on κ_2 and χ_2 one gets $D_L(\omega_2) \sim \omega_2^3$. See [30] for a more general argument along the same line. Thus one expects to observe a pseudo-gap following thermally activated excitations. One effect will deplete the spectrum even further: in the case of a cubic pseudo-gap, the low-frequency spectrum is dominated by states 2 very close to a saddle node bifurcation (at the spinodal). However, once interactions among excitations are taken into account⁶, configurations with such a large density of states near saddle node bifurcation can be shown to be unstable and display avalanche-type events, *i.e.* where the relaxation of one excitation can destabilise others in turn [17]. This effect will increase the pseudo-gap exponent to values larger than three⁷.

As far as the kinetics is concerned, the time scale t_a on which an excitation equilibrates depends on the energy barrier ΔE to go from state 1 to 2. It will occur (neglecting prefactors) when $t_a \gg t_a^* \sim \exp(\Delta E/T)$, *i.e.* its first-passage time. For much larger time scales, the probability of being in the excited states follows a Boltzmann factor $\exp(-E_{12}/T)$ at small T , where E_{12} is the energy difference between the two states. If all states were equilibrated, A_4 would not depend on t_a (*i.e.* $\gamma = 0$). By contrast, if no states were equilibrated A_4 would grow linearly in time. In that respect, our observation of the intermediate case $\gamma \approx 0.2$ is consistent with the notion that there is a broad distribution of barriers, so that on the time scale t_a a fraction of excitations are equilibrated, yet some barriers are still being jumped over for the first time.

For a given gap magnitude ω_c , we expect to find a lower cutoff on the distribution of barriers ΔE (with

⁶Such interactions are relevant even at high temperature near the glass transition [41]. Note that when quenching the system to zero temperature after a reheating, interactions with relaxing vibrational modes may also destabilise excitations which are close to their spinodal.

⁷Interactions between excitations cause a pseudo-gap in the density $P(x) \sim x^\theta$ of excitations within a force x to fail [42, 43]. Near a saddle-node bifurcation, one has $\omega \sim x^{1/4}$ leading to $D_L(\omega) \sim \omega^\alpha$ where $\alpha = 3 + 4\theta$. Empirically $\theta \approx 0.3$ after a slow quench from high temperature (but it is larger for a fast quench) [17], which would lead to an exponent $\alpha \approx 4.2$ consistent with our measurement.

the typical energy difference E_{12} of the associated excitations being of the same order of magnitude). Consider for instance a symmetric double-well in the energy landscape and expand its energy around the maximum: $E(s) = -\frac{1}{2!}\lambda s^2 + \frac{1}{4!}\chi s^4$. It is straightforward to show that in each minimum the frequency of the soft mode scales as $\sqrt{\lambda}$, allowing us to identify for the softest excitations $\lambda \sim \omega_c^2$. Likewise in this example the barrier for the double-well follows $\Delta E \sim \lambda^2 \sim \omega_c^4$. This scaling holds for asymmetric double-wells as well (see Appendix E). Interestingly, our measured activation energy E_a is compatible with this power-law relation, except for the smallest gap (hence less stable glass) that we study⁸.

Overall, this analysis supports the scenario that modes beyond the gap act as a reservoir of excitations, with a broad distribution of barriers presenting a typical cutoff $E_a \sim \omega_c^4$ at low energies.

5 Effects of a thermally filled-up gap on physical properties

5.1 The softening of loading curves is proportional to A_4

We now discuss the practical implications of the preparation dependent amplitude $A_4(T_a, t_a)$ on the mechanical properties of the ultra-stable glass. The relationship between shear transformation and quasi-localized modes was studied in [17] for rapidly quenched glasses. More generally, more stably prepared systems exhibit a steeper loading curve and have a lower density of quasi-localised modes [10, 17]. Here, we show a quantitative relationship between the amplitude of quasi-localised modes A_4 and the effective shear modulus during loading $\mu \equiv \langle \Sigma \rangle / \epsilon$, where ϵ is the imposed shear strain and $\langle \Sigma \rangle$ is the ensemble average of the corresponding shear stress increase⁹. More plasticity leads to a smaller μ .

We measure the stress-strain response in ultra-stable glasses using a quasi-static loading protocol (see Fig. 4(a)). We find that the gapped glasses have the highest effective shear modulus $\mu_0 = \langle \Sigma_0 \rangle / \epsilon$ and it decreases as the gap is filled and A_4 increases (Fig. 4(b)). The reduction of the effective shear mod-

ulus $\Delta\mu(A_4) \equiv \langle \Sigma_0 - \Sigma(A_4) \rangle / \epsilon$ is proportional to A_4 (see Fig. 4(c)) in the range of strains $\epsilon < 0.01$ where it is strain independent.

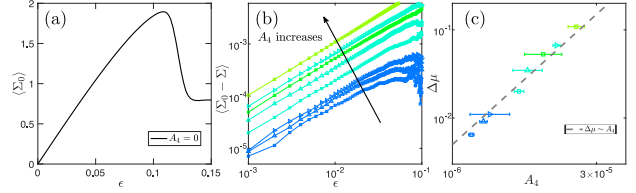


Figure 4. (a) The ensemble averaged shear stress $\langle \Sigma_0 \rangle$ as a function of strain ϵ for our largest gap ($\omega_c = 1.64$). (b) The difference $\langle \Sigma_0 - \Sigma \rangle$ as a function of strain ϵ for different temperature cycles applied to the gapped glass from (a). As observed, the stress decreases as A_4 increases (from bottom to top, $T_a = \{0.15, 0.15, 0.15, 0.2, 0.2, 0.2, 0.23, 0.25\}$ corresponding to $t_a = \{5 \times 10^2, 2 \times 10^3, 10^4, 5 \times 10^2, 2 \times 10^3, 10^4, 5 \times 10^2, 5 \times 10^2\}$, respectively). (c) The decrease in the effective shear modulus $\Delta\mu$ computed at $\epsilon = 10^{-2}$ is proportional to A_4 : the dashed line corresponds to $\Delta\mu \sim A_4$.

5.2 TLS disappear for large gaps

We argue that TLS cannot be observed if a glass presents a large gap. Indeed if the tunneling amplitude is too small, on experimental timescales a single state is visited and TLS properties are not apparent [16]. It is precisely what happens when the gap is large, as barriers are then both larger and wider. To estimate this effect we follow the treatment of soft potential models [44] that solves the Schrödinger equation in potentials described by Eq. (2). For a symmetric double-well, the tunneling time follows $\tau = \hbar\pi/\Delta_0$, where Δ_0 is the splitting energy stemming from quantum tunneling (and \hbar is the reduced Planck constant). Δ_0 is expressed as $\Delta_0 = W \exp(-(\omega_1/\bar{\omega})^3)$ where $W = \hbar(\hbar\chi_1/(96m^2))^{1/3}$ and $\bar{\omega} = (\hbar\chi_1/(2m^2))^{1/3}$ (cf. [44]), with m the particle mass. Thus if $\omega_1 > \omega_c^* \equiv (\ln \frac{\tau W}{\hbar\pi})^{1/3} \bar{\omega}$, TLS are not apparent. In our simulations we find that the median of $\chi_1 \approx 4.6m\omega_D^2/a^2$ (for our largest gap) where a is the inter-particle distance and ω_D is the Debye frequency (see Appendix F for details). Taking estimates in amorphous silicon where $\omega_D \approx k_B 530K/\hbar$ [45], we get $W \approx 0.03\hbar\omega_D$ and $\omega_0 \approx 0.1\omega_D$. Considering the experimentally accessible time scale to be of order $\tau \approx 100s$, at last we estimate $\omega_c^* \approx 0.3\omega_D$. It is of the order of magnitude of our largest gap $\omega_c \approx 0.1\omega_D$.

Suppressing TLS altogether would thus be accomplished by preparing sufficiently stable glasses so as

⁸We observed that for small gaps the assumption that all the excitations are in their energy minimum breaks down, but on the contrary for our largest gap it holds true for about 90% of excitations causing quasi-localised modes. This state of affairs is expected since for very small gaps particles can hardly breathe, and the corresponding gapped states obtained by our protocol are not extremely stable.

⁹Shear stress is measured relative to the initial value at $\epsilon = 0$.

to get $\omega_c > \omega_c^*$. These considerations stay valid even when thermal activation populates the gap and A_4 becomes finite, because quasi-localised modes with low-frequency correspond then to quite asymmetric wells whose barrier height and width (and therefore tunneling amplitude) is still comparable to the estimate above. The presence of a large underlying, thermally populated, gap of quasi-localised modes in ultrastable glasses thus offers an explanation for their lack of TLS [13, 14].

6 Rearrangements involve fewer particles and become string-like at large gaps

We introduce a novel algorithm to decompose the displacement field of a rearrangement into several elementary excitations, which is needed to study how their geometry depends on the gap magnitude. Given a displacement field (induced, in our case, by the thermal cycle), we first consider the particle with maximal displacement, and draw a sphere of radius \tilde{R} around it. Beyond this sphere, all the particle displacements are set to zero (*i.e.* these particles are set back to their initial position in the gapped state), whereas within the sphere the displacements are preserved. Next, we perform with that initial condition a steepest descent of the interaction energy. We find that if \tilde{R} is small, all displacements go back to zero, whereas if \tilde{R} is large, they do not. We consider the smallest \tilde{R} of the latter case, and the displacement field obtained at the end of the corresponding gradient descent defines our first elementary excitation. Next, we subtract this obtained displacement field from the full one, and repeat the entire procedure recursively until no more excitations are found (see Appendix G for details and visual examples).

Given an individual excitation of displacement field $\{\delta\vec{r}_i\}$, we compute, from its associated participation ratio, an estimate of the number of particles involved in this excitation $NP_r \equiv [\sum_i \|\delta\vec{r}_i\|^2]^2 / \sum_i \|\delta\vec{r}_i\|^4$. For each gap magnitude ω_c , we find about 5000 such excitations and report the mean and the median of this observable in Fig. 5(a). We find that the typical number of particles involved in one excitation decreases as ω_c increases. We propose the following rationalisation. The length scale of quasi-localised modes was found to be proportional to the characteristic length scale entering the response to a local dipole [23], as proposed based on a variational arguments in [46]. The length scale ℓ_c entering the dipolar response was ob-

served to decrease as the system moves away from a marginally stable phase and enters a gapped solid phase as $\ell_c \sim 1/\sqrt{\omega_c}$ [47]. The volume of the corresponding mode was shown to go as ℓ_c^2 (independent of the number of dimensions) for elastic networks of springs at rest [46, 47]. Taken together, these results correspond to a number of particles involved in an excitation that decreases with increasing gap as $NP_r \sim 1/\omega_c$. As shown in the inset of Fig. 5(a), this is in reasonable agreement with our observations.

A complementary observable for the geometry is the maximum displacement $\max_i \{\|\delta\vec{r}_i\|\}$ for a given excitation, whose mean and median values for all excitations at a given ω_c are shown in Fig. 5(b). Interestingly, this maximum displacement increases with the gap, and becomes close to the small particle diameter equal to d_0^* .

A direct visualisation of the excitation fields reveals a (presumably related) interesting phenomenon: for our largest gap, the displacements are string-like with several particles exchanging positions, as shown in Fig. 5(c), whereas for smaller gaps they are much more compact and no permutations occur. To quantify this effect, we follow the glass transition literature [4] and measure the distinct part of the Van Hove correlation:

$$G_d(\vec{r}; t) \equiv \frac{1}{N} \left\langle \sum_{i=1}^N \sum_{j(\neq i)}^N \delta(\vec{r} - \vec{r}_j(t) + \vec{r}_i(0)) \right\rangle, \quad (3)$$

where the average is made on all the observed elementary excitations at some given ω_c . It is plotted for our stablest system in Fig. 5(e) after radially averaging. The key observation is the presence of a very sharp peak around $r = 0$, which can only arise from particles replacing each other. Interestingly, if we condition our definition of the Van Hove correlation to large or small particles only, we find that the peak only persists for small particles (in red in Fig. 5(e)). Strings thus correspond to smaller particles navigating in an environment of larger ones.

Next we integrate the peak around $r = 0$ to quantify the number of permuting particles averaged on all elementary excitations:

$$\langle n_p \rangle = \left\langle N \int_0^{r_c} G_d(r, t_a) 4\pi r^2 dr \right\rangle, \quad (4)$$

where r_c is a cutoff that is tuned. We observe that permutations are essentially absent except for the largest considered gap, see Fig. 5(f).

7 Discussion

In summary, we have argued that in gapped glasses, modes beyond the gap act as an excitation reservoir for thermal activation. This effect always destroys the gap and leads to a density of quasi-localised modes $D_L(\omega) \approx A_4(T) \omega^4$. At low temperatures, we found that $A_4 \sim \exp(-E_a(\omega_c)/T)$ where the typical energy scale $E_a(\omega_c)$ is a rapidly increasing function of ω_c . A simple scaling prediction gives $E_a \sim \omega_c^4$, in good agreement with our observations, except for the smallest gap value that we explore. Finally, we observed that as the gap increases, excitations involve fewer and fewer particles and become more and more string-like. The growing length scale of the excitations as $\omega_c \rightarrow 0$ is consistent with the previously identified growing length characterising the elastic response of an amorphous solid near a macroscopic elastic instability [47].

Although our observations were made in ultra-stable states obtained by a specific protocol¹⁰, our arguments on this reservoir effect are much more general. Assuming that this effect is at play in supercooled liquids ties together several unexplained observations, as we now discuss.

Reinterpreting mean-field descriptions of glasses: Goldstein [48] proposed early on that the glass transition takes place near some temperature T_c below which most normal modes become stable. Such an enhanced stability is consistent with the overall elastic stiffening upon cooling apparent in the bulk [49] or local [22] elastic moduli in fragile supercooled liquids. Theoretically, this view is consistent with mean-field models of the glass transition in infinite dimensions – that are closely related to Mode-Coupling Theory – [32, 33], in which the spectrum of the Hessian becomes stable and opens a gap with $\omega_c^2 \sim (T_c - T)$ [34]. Our work suggests a natural way to extend this picture to finite dimensions as sketched in Fig. 1: the gap is decorated by excitations stemming from the reservoir of modes with $\omega \geq \omega_c$. In this approach (i) the excitation density strongly decreases with temperature: away from T_c in the deeply supercooled regime, it should be proportional to $\exp(-E_a(\omega_c(T))/T)$ and (ii) as T decreases, ω_c increases and excitations are less and less extended. Point (i) offers an explanation for the very rapid decay upon cooling of $A_4(T)$

[25, 26], TLS density [27] and shear transformations [10, 50] observed in ultra-stable supercooled liquids. Point (ii) is consistent with the result that TLS [27] and quasi-localised modes [25, 26] present a lower participation ratio upon cooling (such changes of geometry may lead to additional effects on their density¹¹).

Glass transition: The mean-field proposal that supercooled liquids present an effective gap growing upon cooling, leading to a rarefaction of thermally accessible excitations, is consistent with the observation that rearrangements become string-like with more and more particles exchanging positions upon cooling [4, 5] – since we find that excitations at large gap are precisely like that. In our view, why elementary excitations display such a geometry at large gap is yet to be explained¹².

At our lowest temperatures, only one or a few strings get activated, which can only lead to a very partial relaxation of the system. Isolated strings thus belong to the class of β -relaxation in supercooled liquids, as shown in [5], using normal dynamics, for model metallic glasses (molecular and covalent liquids may certainly present other β -relaxation mechanisms governed by the local chemistry, such as dangling bonds). Yet strings may also contribute the α -relaxation of liquids if they are present in sufficient density, at least for the continuously polydisperse ones receiving much attention currently. Indeed they allow for the exchange of particles with distinct radii. Such swap moves are now known to relax the system with great efficiency, so the dynamics should not be slower than the time scale to naturally operate these swaps [53, 54]. The rapid increase of their characteristic low-energy cutoff E_a with growing gap would then contribute to the fragility of liquids.

Note that such views in which activation deep in the supercooled liquid phase is controlled by T_c , contrasts with the usual interpretation of mean-field results in which activation is controlled by an entropy crisis occurring at a lower temperature T_K (the Kauz-

¹¹See [26] for a discussion on quasi-localised modes. Concerning TLS, a smaller participation ratio suggests a higher tunnelling amplitude, which may in turn affect the TLS density.

¹²It was argued within RFOT that strings would exist at intermediate temperatures, [51, 52]. Yet, this analysis is based on the “library of states” picture that describes only rough barriers consisting of many intermediary ones (that must exist between each state of the library), leading to impact rearrangements. This description thus cannot apply to the elementary excitations displaying a single barrier studied here. This picture is explicitly different than our view. In our view, a description of strings should also explain why particles exchange positions.

¹⁰In general to create gapped glasses one needs to use a gradient descent method using swap or equivalently breathing particles up to zero temperature. If instead one uses MD with the normal dynamics to quench from a finite temperature, the gap of magnitude ω_c will be filled by excitations

mann temperature) [32, 33]. The latter is in our opinion ruled out in poly-disperse systems by the recent observation that changes of kinetic rules (such as allowing for swap moves [36]) immensely affect the location of the glass transition, while leaving intact thermodynamic properties [53]. Changes of kinetic rules, however, affect the location of the mode coupling temperature T_c [37, 54], thus pictures of activation based on that temperature are consistent with the observations of swap algorithms.

Effects of rare fluctuations: We have shown that a gap in the density quasi-localised modes cannot exist in finite dimension at finite temperature, due to the thermal activation of their associated excitations. We expect that at least another effect will enter in finite dimension to fill up the gap. In electronic systems that present impurities, the density of states does not vanish in the range of energies where the pure system would, due to rare regions where many impurities are present. This effect leads to the so-called “Lifshitz tail” in the electronic density [55]. In glasses, we expect that aspects of the structure controlling stability, such as coordination and pressure [56, 57], will also fluctuate and lead to rare weaker regions in the materials (we do not see this effect in our breathing particles, whose preparation may lead to an unusually homogeneous material). Such fluctuations will need to be larger and larger as the gap grows to contribute to low-frequency quasi-localised modes, and therefore less likely, leading to a rapidly decaying density of quasi-localised modes with growing gap. These atypical rare regions may have little effect for plasticity or structural relaxation near the glass transition, but may be important in affecting the density of TLS. It would thus be interesting in the future to study glasses of controlled inhomogeneity to separate rare fluctuations in the structural disorder from the ‘excitations reservoir’ effect introduced here.

Acknowledgements

We would like to thank L. Berthier, G. Biroli, C. Cammarota, D. Khomenko, C. Liu, V. Lubchenko, M. Müller, M. Ozawa, C. Scalliet, P. Wolynes and F. Zamponi for fruitful discussions, as well as G. Kapteijns and E. Lerner for discussions and numerical support at the beginning. T.G. acknowledges support from The Netherlands Organisation for Scientific Research (NWO) by a NWO Rubicon Grant 680-50-1520 and from the Swiss National Science Foundation (SNSF) by the SNSF Ambizione Grant PZ00P2_185843. E.A. acknowledges sup-

port from the SNSF by the SNSF Ambizione Grant PZ00P2_173962, and M.W. by the Simons Foundation Grant (#454953 Matthieu Wyart) and from the SNSF under Grant No. 200021-165509.

References

- [1] W.A. Phillips. Tunneling states in amorphous solids. *J. Low Temp. Phys.*, 7(3-4):351–360, 1972.
- [2] P.W. Anderson, B.I. Halperin, and C.M. Varma. Anomalous low-temperature thermal properties of glasses and spin glasses. *Philos. Mag.*, 25(1):1–9, 1972.
- [3] W.A. Phillips. Two-level states in glasses. *Reports Prog. Phys.*, 50(12):1657–1708, 1987.
- [4] C. Donati, J.F. Douglas, W. Kob, S.J. Plimpton, P.H. Poole, and S.C. Glotzer. Stringlike Cooperative Motion in a Supercooled Liquid. *Phys. Rev. Lett.*, 80(11):2338–2341, 1998.
- [5] H.-B. Yu, R. Richert, and K. Samwer. Structural rearrangements governing Johari-Goldstein relaxations in metallic glasses. *Sci. Adv.*, 3(11):e1701577, 2017.
- [6] C. Maloney and A. Lemaitre. Subextensive Scaling in the Athermal, Quasistatic Limit of Amorphous Matter in Plastic Shear Flow. *Phys. Rev. Lett.*, 93(1):016001, 2004.
- [7] A. Heuer. Exploring the potential energy landscape of glass-forming systems: from inherent structures via metabasins to macroscopic transport. *J. Phys. Condens. Matter*, 20(37):373101, 2008.
- [8] A.S. Argon. Plastic deformation in metallic glasses. *Acta Metall.*, 27(1):47–58, 1979.
- [9] D. Vandembroucq and S. Roux. Mechanical noise dependent aging and shear banding behavior of a mesoscopic model of amorphous plasticity. *Phys. Rev. B*, 84(13):134210, 2011.
- [10] M. Ozawa, L. Berthier, G. Biroli, A. Rosso, and G. Tarjus. Random critical point separates brittle and ductile yielding transitions in amorphous materials. *Proc. Natl. Acad. Sci.*, 115(26):6656–6661, 2018.
- [11] M. Popović, T.W.J. de Geus, and M. Wyart. Elastoplastic description of sudden failure in athermal amorphous materials during quasistatic loading. *Phys. Rev. E*, 98(4):040901(R), 2018.
- [12] M.D. Ediger, C.A. Angell, and S.R. Nagel. Supercooled Liquids and Glasses. *J. Phys. Chem.*, 100(31):13200–13212, 1996.
- [13] D.R. Queen, X. Liu, J. Karel, T.H. Metcalf, and F. Hellman. Excess Specific Heat in Evaporated Amorphous Silicon. *Phys. Rev. Lett.*, 110(13):135901, 2013.
- [14] T. Pérez-Castañeda, C. Rodríguez-Tinoco, J. Rodríguez-Viejo, and M.A. Ramos. Suppression of tunneling two-level systems in ultrastable glasses of indomethacin. *Proc. Natl. Acad. Sci.*, 111(31):11275–11280, 2014.
- [15] J.M. Martinis, K.B. Cooper, R. McDermott, M. Steffen, M. Ansmann, K.D. Osborn, K. Cicak, S. Oh, D.P. Pappas, R.W. Simmonds, and C.C. Yu. Decoherence in Josephson Qubits from Dielectric Loss. *Phys. Rev. Lett.*, 95(21):210503, 2005.
- [16] D. A. Parshin, H. R. Schober, and V.L. Gurevich. Vibrational instability, two-level systems, and the boson peak in glasses. *Phys. Rev. B*, 76(6):064206, 2007.
- [17] W. Ji, M. Popović, T.W.J. de Geus, E. Lerner, and M. Wyart. Theory for the density of interacting quasilocalized modes in amorphous solids. *Phys. Rev. E*, 99(2):023003, 2019.
- [18] H.R. Schober, C. Oligschleger, and B.B. Laird. Low-frequency vibrations and relaxations in glasses. *J. Non. Cryst. Solids*, 156-158:965–968, 1993.

- [19] M. Baity-Jesi, V. Martín-Mayor, G. Parisi, and S. Perez-Gaviro. Soft Modes, Localization, and Two-Level Systems in Spin Glasses. *Phys. Rev. Lett.*, 115(26):267205, 2015.
- [20] E. Lerner, G. Düring, and E. Bouchbinder. Statistics and Properties of Low-Frequency Vibrational Modes in Structural Glasses. *Phys. Rev. Lett.*, 117(3):035501, 2016.
- [21] H. Mizuno, H. Shiba, and A. Ikeda. Continuum limit of the vibrational properties of amorphous solids. *Proc. Natl. Acad. Sci.*, 114(46):E9767–E9774, 2017.
- [22] E. Lerner and E. Bouchbinder. A characteristic energy scale in glasses. *J. Chem. Phys.*, 148(21):214502, 2018.
- [23] M. Shimada, H. Mizuno, M. Wyart, and A. Ikeda. Spatial structure of quasilocated vibrations in nearly jammed amorphous solids. *Phys. Rev. E*, 98(6):060901, 2018.
- [24] C. Scalliet, L. Berthier, and F. Zamponi. Nature of excitations and defects in structural glasses. *Nat. Commun.*, 10(1):5102, 2019.
- [25] L. Wang, A. Ninarello, P. Guan, L. Berthier, G. Szamel, and E. Flenner. Low-frequency vibrational modes of stable glasses. *Nat. Commun.*, 10(1):26, 2019.
- [26] C. Rainone, E. Bouchbinder, and E. Lerner. Pinching a glass reveals key properties of its soft spots. *Proc. Natl. Acad. Sci.*, 117(10):5228–5234, 2020.
- [27] Dmytro Khomenko, Camille Scalliet, Ludovic Berthier, David R Reichman, and Francesco Zamponi. Depletion of two-level systems in ultrastable computer-generated glasses. *Physical Review Letters*, 124(22):225901, 2020.
- [28] V. Lubchenko and P.G. Wolynes. Intrinsic Quantum Excitations of Low Temperature Glasses. *Phys. Rev. Lett.*, 87(19):195901, 2001.
- [29] V.L. Gurevich, D.A. Parshin, and H.R. Schober. Anharmonicity, vibrational instability, and the Boson peak in glasses. *Phys. Rev. B*, 67(9):094203, 2003.
- [30] V. Gurarie and J.T. Chalker. Bosonic excitations in random media. *Phys. Rev. B*, 68(13):134207, 2003.
- [31] A. Cavagna. Supercooled liquids for pedestrians. *Phys. Rep.*, 476(4-6):51–124, 2009.
- [32] V. Lubchenko and P.G. Wolynes. Theory of Structural Glasses and Supercooled Liquids. *Annu. Rev. Phys. Chem.*, 58(1):235–266, 2007.
- [33] G. Biroli and J.-P. Bouchaud. The Random First-Order Transition Theory of Glasses: a critical assessment. *Struct. Glas. Supercooled Liq. Theory, Exp. Appl.*, pages 31–113, 2009.
- [34] G. Parisi. On the origin of the boson peak. *J. Phys. Condens. Matter*, 15(11):S765–S774, 2003.
- [35] G. Kapteijns, W. Ji, C. Brito, M. Wyart, and E. Lerner. Fast generation of ultrastable computer glasses by minimization of an augmented potential energy. *Phys. Rev. E*, 99(1):012106, 2019.
- [36] A. Ninarello, L. Berthier, and D. Coslovich. Models and Algorithms for the Next Generation of Glass Transition Studies. *Phys. Rev. X*, 7(2):021039, 2017.
- [37] C. Brito, E. Lerner, and M. Wyart. Theory for Swap Acceleration near the Glass and Jamming Transitions for Continuously Polydisperse Particles. *Phys. Rev. X*, 8(3):031050, 2018.
- [38] E. Lerner and E. Bouchbinder. Effect of instantaneous and continuous quenches on the density of vibrational modes in model glasses. *Phys. Rev. E*, 96(2):020104, 2017.
- [39] L. Berthier, E. Flenner, C.J. Fullerton, C. Scalliet, and M. Singh. Efficient swap algorithms for molecular dynamics simulations of equilibrium supercooled liquids. *J. Stat. Mech. Theory Exp.*, 2019(6):064004, 2019.
- [40] E. Bitzek, P. Koskinen, F. Gähler, M. Moseler, and P. Gumbsch. Structural Relaxation Made Simple. *Phys. Rev. Lett.*, 97(17):170201, 2006.
- [41] A. Lemaître. Structural Relaxation is a Scale-Free Process. *Phys. Rev. Lett.*, 113(24):245702, 2014.
- [42] J. Lin, A. Saade, E. Lerner, A. Rosso, and M. Wyart. On the density of shear transformations in amorphous solids. *EPL (Europhys. Lett.)*, 105(2):26003, 2014.
- [43] J. Lin and M. Wyart. Mean-Field Description of Plastic Flow in Amorphous Solids. *Phys. Rev. X*, 6(1):011005, 2016.
- [44] D.A. Parshin. Soft potential model and universal properties of glasses. *Phys. Scr.*, T49A(T49A):180–185, 1993. doi: 10.1088/0031-8949/1993/T49A/030.
- [45] M. Mertig, G. Pompe, and E. Hegenbarth. Specific heat of amorphous silicon at low temperatures. *Solid State Commun.*, 49(4):369–372, 1984. doi: 10.1016/0038-1098(84)90589-1.
- [46] L. Yan, E. DeGiuli, and M. Wyart. On variational arguments for vibrational modes near jamming. *EPL (Europhys. Lett.)*, 114(2):26003, 2016.
- [47] E. Lerner, E. DeGiuli, G. Düring, and M. Wyart. Breakdown of continuum elasticity in amorphous solids. *Soft Matter*, 10(28):5085, 2014.
- [48] M. Goldstein. Viscous Liquids and the Glass Transition: A Potential Energy Barrier Picture. *J. Chem. Phys.*, 51(9):3728–3739, 1969.
- [49] T. Hecksher and J.C. Dyre. A review of experiments testing the shoving model. *J. Non. Cryst. Solids*, 407:14–22, 2015.
- [50] Y. Jin, P. Urbani, F. Zamponi, and H. Yoshino. A stability-reversibility map unifies elasticity, plasticity, yielding, and jamming in hard sphere glasses. *Sci. Adv.*, 4(12):eaat6387, 2018.
- [51] J.D. Stevenson, J. Schmalian, and P.G. Wolynes. The shapes of cooperatively rearranging regions in glass-forming liquids. *Nat. Phys.*, 2(4):268–274, 2006.
- [52] J.D. Stevenson and P.G. Wolynes. A universal origin for secondary relaxations in supercooled liquids and structural glasses. *Nat. Phys.*, 6(1):62–68, 2010.
- [53] M. Wyart and M.E. Cates. Does a Growing Static Length Scale Control the Glass Transition? *Phys. Rev. Lett.*, 119(19):195501, 2017.
- [54] H. Ikeda, F. Zamponi, and A. Ikeda. Mean field theory of the swap Monte Carlo algorithm. *J. Chem. Phys.*, 147(23):234506, 2017.
- [55] I.M. Lifshitz. Energy spectrum structure and quantum states of disordered condensed systems. *Sov. Phys. Uspekhi*, 7(4):549–573, 1965. doi: 10.1070/PU1965v007n04ABEH003634.
- [56] S. Alexander. Amorphous solids: their structure, lattice dynamics and elasticity. *Phys. Rep.*, 296(2-4):65–236, 1998. doi: 10.1016/S0370-1573(97)00069-0.
- [57] M. Wyart, L.E. Silbert, S.R. Nagel, and T.A. Witten. Effects of compression on the vibrational modes of marginally jammed solids. *Phys. Rev. E*, 72(5):051306, 2005.
- [58] H.J.C. Berendsen, J.P.M. Postma, W.F. van Gunsteren, A. DiNola, and J.R. Haak. Molecular dynamics with coupling to an external bath. *J. Chem. Phys.*, 81(8):3684–3690, 1984.

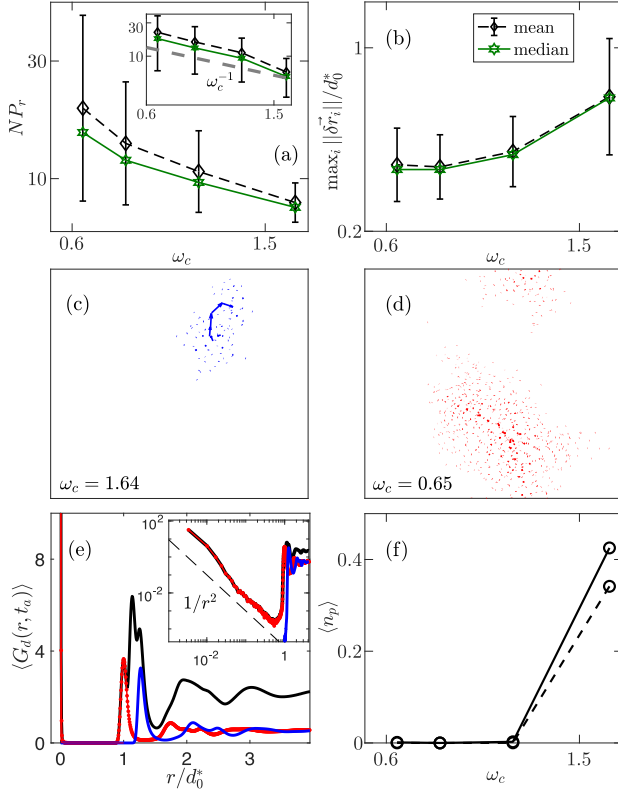


Figure 5. (a) Mean (dashed black) and median (green) of the number of particles NP_r involved in an individual excitation *vs* ω_c at $t_a = 500$ (at the lowest temperature we probe for each gap). The error bars stand for the standard deviation of NP_r which indicates that the distribution of NP_r is broader for smaller ω_c . (b) Mean (dashed black) and median (green) of the displacement norm of the most mobile particle in an excitation, as a function of ω_c . d_0^* is the most frequent diameter of the smaller particles ($d_0^* = \{0.738, 0.918, 0.963, 0.988\}$ for the different ω_c). (c)-(d) Thermally induced rearrangement, respectively for our largest ($\omega_c = 1.64$) and smallest ($\omega_c = 0.65$) gaps, projected on the xy plane. (e) Ensemble and radially averaged (on all observed excitations) Van Hove correlation function $G_d(r, t_a)$ computed for all (in black and having largest G_d at large r), only small (red dotted) or only large (blue) particles for $\omega_c = 1.64$. The peak around $r = 0$ corresponds to permutations of particles. The black and red curves overlap, indicating that permutations only occur on small particles. (f) Average number of permutations $\langle n_p \rangle$ *vs* ω_c , for two different cutoff distances $r_c/d_0^* = \{0.025, 0.05\}$ (dashed and solid, respectively).

A Parameters & Key quantities

K	10^2	10^3	3×10^3	10^4
ω_c	1.65	1.19	0.85	0.65
n	4000	4000	2000	3000
N	8000	8000	8000	8000
ϕ	0.62	0.74	0.77	0.79
$\langle V \rangle$	3722.0 ± 0.3	7303.9 ± 0.7	8607.2 ± 0.9	9356 ± 1
ρ	2.15	1.10	0.93	0.86
T_p	0.2	0.39	0.44	0.49
t_p	$1e4$	$1e4$	$1e4$	$1e4$
T_c	0.304	0.484	0.525	0.572
T_a	{0.15, 0.20, 0.23, 0.25, 0.27, 0.30, 0.40}	{0.07, 0.10, 0.20, 0.30, 0.39, 0.50, 0.60, 0.80}	{0.03, 0.05, 0.1}	{0.03, 0.05, 0.10, 0.20, 0.30, 0.49, 0.60, 0.80}
t_a	{500, 2000, 10000}	{100, 500, 2000}	{500}	{100, 500, 2000}
E_a	0.66 ± 0.08	0.15 ± 0.03	0.042 ± 0.016	0.03 ± 0.007
γ	0.2	0.05	-	0.003
$\langle n_e \rangle$	0.65	0.89	1.2	3.2

Notice that $\phi \equiv \sum_{i=1}^N \frac{4}{3}\pi R_i^3/V$ is the packing fraction; and that $\langle V \rangle$ is the ensemble average volume (and the uncertainty its standard deviation). The average number of excitations per realisation $\langle n_e \rangle$ has been obtained with $t_a = 500$ at the lowest T_a we probed for each K . T_c is obtained from the relation: relaxation time $\sim (T - T_c)^{-\nu}$ [31], where ν is also a fit parameter. Lengths (\vec{r} , R_i and L) are shown in the unit of d_0 (or the most frequent diameter of small particles d_0^* , if so indicated): the diameter of an initially small particle. Energies (E_a) are expressed in the unit of ε that is the prefactor of the pair interaction potential (see below). Temperature (T_p , T_a , and T_c) is in the unit of ε/k_B . Time (t_p , t_a , and ω^{-1}) is shown in the unit of t_0 where $t_0 \equiv \sqrt{md_0^2/\varepsilon}$.

Detecting a rearrangement

To detect if reheating with a temperature T_a for a duration of t_a has led to a rearrangement we consider the ratio of the norm and the participation ratio of the displacement field:

$$\mathcal{I} \equiv \frac{\|\delta\vec{r}_i\|}{P_r(\delta\vec{r}_i)} \quad (5)$$

where $\|\delta\vec{r}_i\|$ is the Euclidean norm of the particle displacement field, $\delta\vec{r}_i$, between the quenched states before and after reheating, and its participation ratio

$$P_r(\delta\vec{r}_i) \equiv \frac{(\sum_i \|\delta\vec{r}_i\|^2)^2}{N \sum_i \|\delta\vec{r}_i\|^4} \quad (6)$$

If a rearrangement results from reheating, the norm of the displacement field is finite (typically $10^{-3} - 10^{-2}$) and participation ratio in the order of $10^{-3} - 10^{-2}$. In contrast, if there was no rearrangement, the norm of the displacement field is of the order of the numerical precision (10^{-6}) and the participation ratio is of order one. We distinguish the two cases using a threshold. We define that a rearrangement has taken place if $\mathcal{I} > 10^{-3}$. Note that the distributions of \mathcal{I} corresponding to the two cases are clearly separated.

B Molecular dynamics

Sample preparation: ‘breathing’ dynamics

We study a three-dimensional periodic particle system of $N = 8000$ particles, that is characterised by the grand potential

$$\mathcal{U} = \sum_{i < j} \varphi(r_{ij}, R_i, R_j) + \sum_i \mu(R_i, R_i^{(0)}) \quad (7)$$

where φ is a purely repulsive inverse power-law potential, defined

$$\varphi(r_{ij}, R_i, R_j) = \begin{cases} \varepsilon \left[\left(\frac{R_{ij}}{r_{ij}} \right)^{10} + \sum_{p=0}^3 c_{2p} \left(\frac{r_{ij}}{R_{ij}} \right)^{2p} \right], & \frac{r_{ij}}{R_{ij}} \leq r_c \\ 0, & \frac{r_{ij}}{R_{ij}} > r_c \end{cases} \quad (8)$$

with r_c is the cutoff distance, $R_{ij} \equiv R_i + R_j$ (two times the average particle radius), and $r_{ij} \equiv \|\vec{r}_{ij}\| \equiv \|\vec{r}_i - \vec{r}_j\|$ (the Euclidean norm of the distance vector separating particles i and j). c_{2p} is a constant that makes φ continuous up to the third derivative at r_c . Furthermore,

$$\mu(R_i, R_i^{(0)}) = \frac{K}{2} \left(1 - \frac{R_i^{(0)}}{R_i} \right)^2 \left(R_i^{(0)} \right)^2 \quad (9)$$

is a chemical potential that allows a particle to change its size from its initial value $R_i^{(0)}$ at an energetic cost that scales with a modulus K . For $K = \infty$ it is impossible for a particle to change its radius, while it becomes easier as $K \rightarrow 0$. The initial particle radii are bi-disperse, in a 50:50 mixture. In particular, one, randomly selected, half of the particles has $R_i^{(0)} = 0.5d_0$ and the other half has $R_i^{(0)} = 0.7d_0$ (where d_0 sets the unit of length of our system).

Sample preparation proceeds by instantaneously heating the initial random configuration to a temperature T_p and keeping it at this temperature for a certain time t_p under the constraint of a fixed pressure $p = 20.0$ (in units of ε/d_0^3). We then instantaneously quench the system to zero temperature by minimising the grand potential. See algorithmic details below.

Activation by temperature: normal dynamics

We proceed by fixing the particle size, which corresponds to a potential energy

$$U = \sum_{i < j} \varphi(r_{ij}, R_i, R_j) \quad (10)$$

(see Eq. (8) for the definition of φ). We then gently heat the system configuration to a certain ‘activation temperature’ T_a (at a heating rate $T_a/(10 t_0)$), and keep the sample at T_a for a total duration t_a . Thereafter we instantaneously quench the sample to zero temperature. Algorithmic details are listed below.

Molecular dynamics algorithm

We run molecular dynamics, whereby the particle dynamics are given by Newton’s equation of motion with the gradient of the potential energy on a particle as driving force. Time is discretised in steps of Δt using the standard velocity Verlet algorithm. The temperature and pressure are controlled using a Berendsen thermostat [58], where the temperature is defined as the total kinetic energy $\sum_i m \|\dot{\vec{r}}_i\|^2/2$ (where $\dot{\bullet}$ refers to the time derivative). Note that during preparation the kinetic energy is $\sum_i (m \|\dot{\vec{r}}_i\|^2 + \dot{R}_i^2)/2$. We use the ‘FIRE’ algorithm [40] to quench the systems.

For completeness we report that $r_c = 1.48 d_0$, $\varepsilon = 1$, $m = 1$, $d_0 = 1$, and $\Delta t = 0.005$. Furthermore $c_0 = -1.1106337662511798$, $c_2 = 1.2676152372297065$, $c_4 = -0.4960406072849212$, $c_6 = 0.0660511826415732$; see Supplemental Material of [38].

C Sample preparation

We choose T_p and t_p to empirically generate a configuration in the lowest possible energetic state in terms of the mean interaction energy $\langle u \rangle = \langle U \rangle / N$ (averaged on an ensemble of $n = 10$ samples). In particular, we set $t_p = 10^4$ (the highest value we can practically reach, with each sample taking eight CPU hours to prepare). We manually optimise T_p as reported in Fig. 6. Note that we verify that the T_p at which we find the optimum, is robust in terms of preparation duration t_p , by comparing our results to those for $t_p = 500$ (dashed line in Fig. 6). Furthermore, the reader is reminded that although the particle size distribution depends on temperature while still at T_p , the final particle size distribution at zero temperature is independent of T_p . Note that our ‘breathing’ dynamics (at small K) are quite efficient to prepare samples in a low potential energy state. We verify this by preparing an ensemble (again $n = 10$, but with $N = 2000$ particles) with normal dynamics and a slow quench rate. We plot the potential energy $\langle u \rangle$ at different temperatures in Fig. 7. In all cases $\langle u \rangle$ at $T = 0$ is higher than that for the sample prepared using ‘breathing’ dynamics, which was prepared at a fraction of the computational costs (sample preparation is a factor of 2000 faster using ‘breathing’ dynamics).

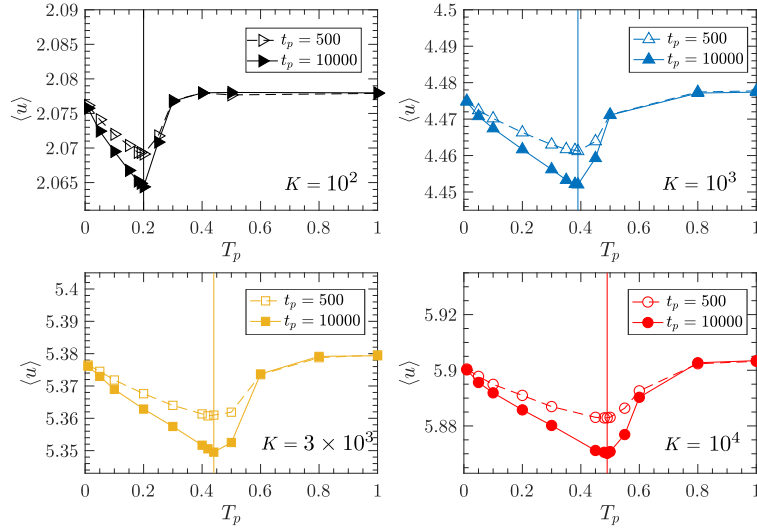


Figure 6. Mean interaction potential energy $\langle u \rangle$ after sample preparation with ‘breathing’ dynamics for varying parent temperature T_p and two different waiting times t_p . The different panels correspond to different K as indicated. The selected temperature T_p for which the potential energy is lowest for the largest practically reachable $t_p = 10^4$ is indicated using vertical lines (see Appendix A for numeric values).

D Measurement of quasi-localised modes

Spectrum of the Hessian

We extract the Hessian (or stiffness matrix) – the second derivative of interaction energy – as follows

$$\mathcal{H}_{ij} \equiv \frac{\partial^2 U}{\partial \vec{r}_i \partial \vec{r}_j} = -\frac{d^2 \varphi(r_{ij})}{dr_{ij}^2} \frac{\vec{r}_{ij} \vec{r}_{ij}}{r_{ij}^2} - \frac{d\varphi(r_{ij})}{dr_{ij}} \frac{1}{r_{ij}} \left(\mathcal{I} - \frac{\vec{r}_{ij} \vec{r}_{ij}}{r_{ij}^2} \right) \quad (11)$$

for $i \neq j$. The diagonal

$$\mathcal{H}_{ii} = -\sum_{i \neq j} \mathcal{H}_{ij} \quad (12)$$

due to translation symmetry. Note that \mathcal{H}_{ij} is a second-order tensor, and that $\mathcal{I} = \delta_{\alpha\beta} \vec{e}_\alpha \vec{e}_\beta$ is a second order unit tensor. We then diagonalise the Hessian, leading to N eigenvalues λ and corresponding eigenmodes $\vec{\Phi}_i$.

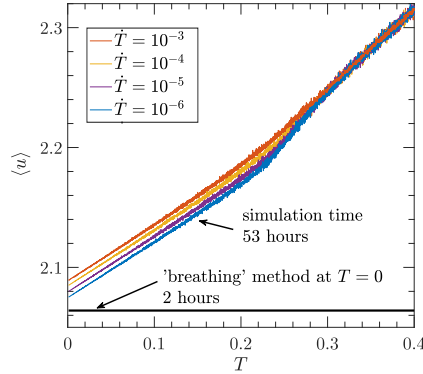


Figure 7. Mean interaction potential energy as obtained by sample preparation using ‘breathing’ dynamics (at $T = 0$ for $K = 10^2$, $t_p = 10^4$, and $T_p = 0.2$, in black) and using normal dynamics at different cooling rates (cooling from $T = 0.4$) as indicated in the legend. Note that in both cases the ensemble comprises $n = 10$ samples, but that normal dynamics are run using smaller than usual samples comprising $N = 2000$ particles ($N = 8000$ is used throughout). We verify the representativeness of these smaller samples using $N = 8000$ for $\dot{T} = 10^{-3}$, shown using a dashed red line (that indeed coincides with the solid red line for $N = 2000$). The required CPU time to run the entire simulation with $N = 2000$ particles is indicated. From bottom to top, \dot{T} increases. Note that for our ‘breathing’ dynamics the time has been divided by four to correct for the difference in system size.

Because all particles have a mass $m = 1$ the corresponding N eigenfrequencies are

$$\omega \equiv \sqrt{\lambda} \quad (13)$$

We finally represent the spectrum of the Hessian as

$$D(\omega) = \frac{1}{3N-3} \sum_{k=1}^{3N-3} \delta(\omega - \omega_k) \quad (14)$$

Density of quasi-localised modes

The density of quasi-localised modes, $D_L(\omega)$, follows from the spectrum of the Hessian in Eq. (14) by filtering plane waves that have a frequency $\omega_e < \omega_c$ (where ω_c is defined below). We identify these plane waves by their signature in participation ratio

$$P_r(\vec{\Phi}_i) \equiv \frac{(\sum_i \|\vec{\Phi}_i\|^2)^2}{N \sum_i \|\vec{\Phi}_i\|^4} \quad (15)$$

Plane waves thereby have $P_r \approx 2/3$, while quasi-localised modes have $P_r \ll 1$.

In practice, most of our samples have no plane waves below ω_c , rendering filtering obsolete. In fact, we only apply filtering after sample preparation for $K = \{10^2, 10^3\}$. Since we empirically observe the plane waves to be well separated from the quasi-localised modes in terms of frequency, we remove them by removing the first $3 + 12$ eigenmodes of each realisation for $K = 10^3$ and $3 + 12 + 24$ eigenmodes of each realisation for $K = 10^2$, corresponding the 3 translational modes and the first (two) bands of plane waves¹³. Note that $D_L(\omega)$ is not renormalised after filtering of plane waves.

We emphasise that in all other measurements $D_L(\omega) = D(\omega)$ at low frequency.

Protocol to measure ω_c

We measure the gap frequency ω_c – the frequency of the first quasi-localised mode. To measure ω_c , we assert that the density of soft quasi-localised modes follows

$$D_L(\omega) \sim (\omega - \omega_c)^\zeta \quad (16)$$

¹³For $K = 10^3$, $\omega_e = 1.30 \pm 0.02$, and for $K = 10^2$, $\omega_e = \{1.26 \pm 0.03, 1.73 \pm 0.05\}$ (where the uncertainty refers to the standard deviation).

at low frequency ω . We then move ω_c until the power law is most obvious at low ω , as shown in Fig. 8. We then visually extract the power ζ and check that it and the extracted ω_c are consistent with extreme-value statistics. In particular, we expect

$$\omega'_{\min} - \omega_c \sim (n')^{-1/(1+\zeta)} \quad (17)$$

where ω'_{\min} is the frequency of the softest quasi-localised mode in an ensemble of n' realisations chosen as a random subset of our ensemble of n realisations. We consider $\bar{\omega}'_{\min}$ the average of lowest three realisations (out of n' realisations). Indeed, our extracted ω_c is consistent with this scaling, as shown in the insets of Fig. 8. In addition, we check that ω_c is robust to a change of system size (shown in Fig. 8).

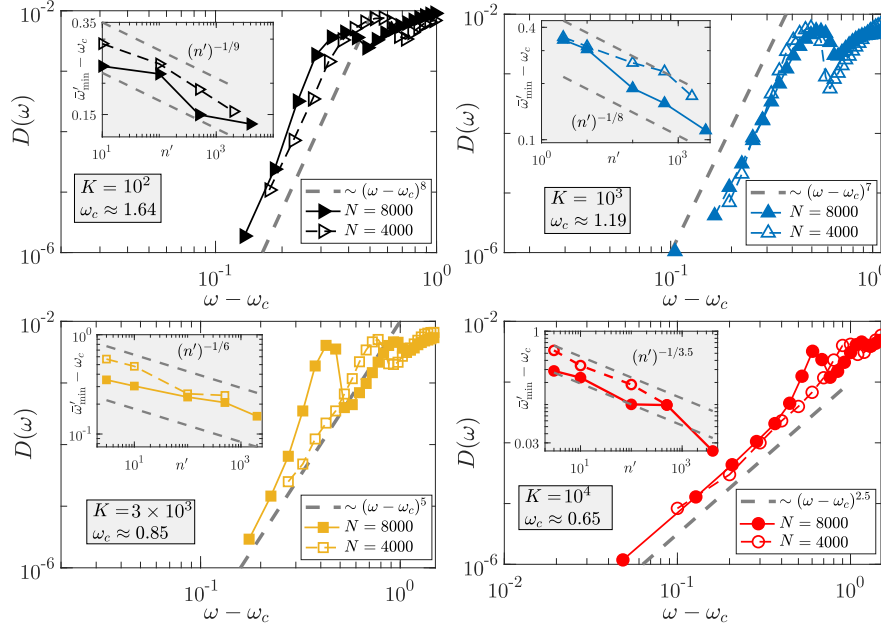


Figure 8. Fit of ω_c by asserting the power law scaling in Eq. (16) and check by extreme value statistics as in Eq. (17) (insets), for all considered K .

Protocol to fit A_4

A_4 is extracted from $D_L(\omega)$ by fitting

$$D_L(\omega) = A_4 \omega^4 \quad (18)$$

(i.e. Eq. (1)) for frequencies below the first plane wave (for $K = 10^2$) and for frequencies below ω_c (for $K = 10^3$, 3×10^3 , and 10^4). Note that consequently $D_L(\omega) = D(\omega)$ in the relevant frequency range for all these measurements. The mean and the error of A_4 follow as the mean and standard deviation of $\{\ln D(\omega_i) - 4 \ln \omega_i\}$ where ω_i corresponds to the position of the bins of $D(\omega)$.

We verify that the value of A_4 that we fit is robust to a mild decrease of system size (using $n = 2000$ realisations of $N = 4000$ particles, compared to an ensemble of $n = 4000$ realisations of $N = 8000$ particles). We find that both the density of soft quasi-localised modes and the extracted A_4 are robust to the change of system size, as reported in Fig. 9.

Protocol to fit E_a and γ

Our protocol to fit E_a and extract γ consists of two steps. 1) We first collapse the curves of $A_4(T_a)$ for different t_a . Thereto we shift the horizontal axis of e.g. Fig. 3(b) in accordance with assuming a functional dependence

$$A_4 = A_4 \left(t_a^\gamma e^{-E_a/T_a} \right) \quad (19)$$

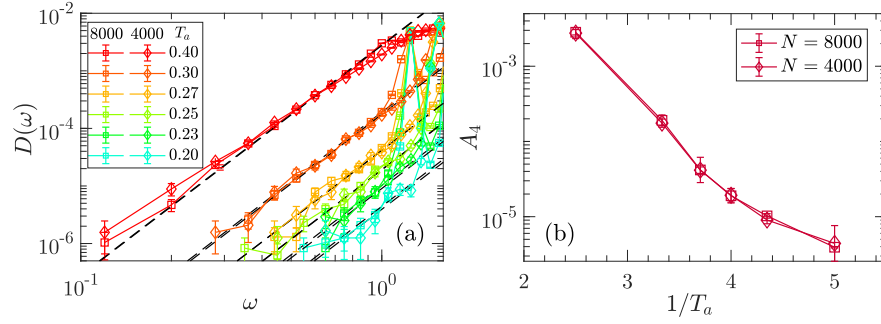


Figure 9. (a) $D(\omega)$ for different system sizes N and different activation temperatures T_a (as indicated in the legend T_a increases from bottom to top). (b) A_4 fitted on (a) as a function of $1/T_a$. Both plots are for $K = 10^2$ and $t_a = 500$.

until the curves for different t_a collapse to a single curve (e.g. Fig. 3(c)), by optimising the ratio γ/E_a . 2) On the master curve we next fit E_a of low T_a . Since we know the ratio γ/E_a , the fitted value of E_a gives us direct access to E_a . Specifically, we fit $\ln(A_4)$ vs $1/T_a - \gamma/E_a \ln t_a$ using linear regression to get E_a and its error at low T_a (the lowest 5 data points in Fig. 3(c)).

Results for different K

In Fig. 10 we show the collapse of different waiting times t_a and the fit of E_a at low T_a for all ensembles that are not shown in the main text (notably Fig. 3). Note that for $K = 3 \times 10^3$ we extract E_a by directly fitting for low T_a for a single t_a .

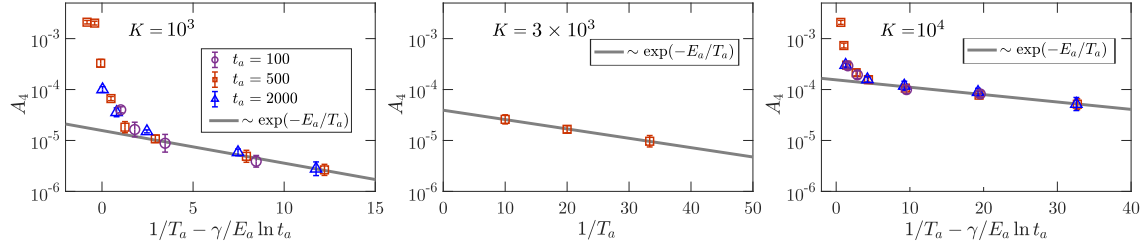


Figure 10. Fitting of E_a and γ for all K not shown in the main text. The fitted values are reported in Appendix A.

Robustness of E_a

In Fig. 11 we verify that the consistency with $E_a \sim \omega_c^4$ is robust to a different measure of the softest quasi-localised mode after sample preparation. In particular, we compare with ω_{\min} .

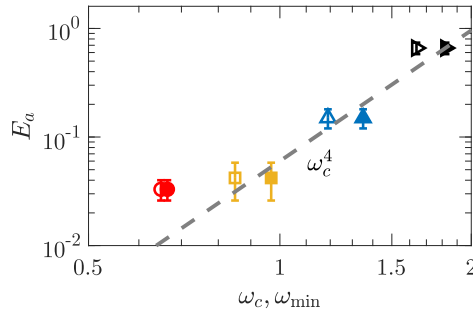


Figure 11. E_a as a function of ω_c (open markers) or as a function of ω_{\min} (solid markers).

E The Jacobian of the transformation from $(\lambda_1, \kappa_1, \chi_1)$ to $(\lambda_2, \kappa_2, \chi_2)$

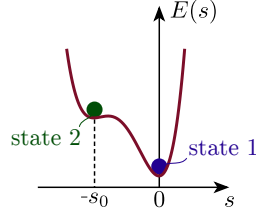


Figure 12. Double-well potential.

The potential around the state 1 is given by:

$$E(s) = \frac{1}{2!}\lambda_1 s^2 + \frac{1}{3!}\kappa_1 s^3 + \frac{1}{4!}\chi_1 s^4 + \text{constant} \quad (20)$$

with the joint distribution $P(\lambda_1, \kappa_1, \chi_1)$ that is strictly zero at $\lambda_1 < \omega_c^2$ and smooth above ω_c^2 . $\chi_1 > 0$. Without loss of generality, we let $\kappa_1 > 0$. For the new minimum, state 2, the potential reads:

$$E(s) = \frac{1}{2!}\lambda_2 (s + s_0)^2 + \frac{1}{3!}\kappa_2 (s + s_0)^3 + \frac{1}{4!}\chi_2 (s + s_0)^4 + \text{constant} \quad (21)$$

where s_0 is the shift along s , see Fig. 12; and the corresponding joint distribution is $P(\lambda_2, \kappa_2, \chi_2)$. The convention $\kappa_1 > 0$ leads to the position $s_2 = -s_0$ of state 2 smaller than 0.

The relation between two sets of coefficients $\lambda_1, \kappa_1, \chi_1$ and $\lambda_2, \kappa_2, \chi_2$ is

$$\begin{cases} \chi_1 = \chi_2 \\ \kappa_1 = \kappa_2 + \chi_2 s_0 \\ \lambda_1 = \lambda_2 + \kappa_2 s_0 + \frac{1}{2}\chi_2 s_0^2 \end{cases} \quad (22)$$

where s_0 as a function of $(\lambda_2, \kappa_2, \chi_2)$ follows from the fact that the linear term vanishes in Eqs. (20) and (21). In particular,

$$6\lambda_2 + 3\kappa_2 s_0 + \chi_2 s_0^2 = 0 \quad (23)$$

The joint distribution $P(\lambda_2, \kappa_2, \chi_2)$ is given by

$$P(\lambda_2, \kappa_2, \chi_2) = \left| \det \left(\frac{d\lambda_1 d\kappa_1 d\chi_1}{d\lambda_2 d\kappa_2 d\chi_2} \right) \right| P(\lambda_1, \kappa_1, \chi_1) \quad (24)$$

where

$$\left| \det \left(\frac{d\lambda_1 d\kappa_1 d\chi_1}{d\lambda_2 d\kappa_2 d\chi_2} \right) \right| \equiv \left| \det \left(\begin{bmatrix} \frac{\partial \lambda_1}{\partial \lambda_2} & \frac{\partial \lambda_1}{\partial \kappa_2} & \frac{\partial \lambda_1}{\partial \chi_2} \\ \frac{\partial \kappa_1}{\partial \lambda_2} & \frac{\partial \kappa_1}{\partial \kappa_2} & \frac{\partial \kappa_1}{\partial \chi_2} \\ \frac{\partial \chi_1}{\partial \lambda_2} & \frac{\partial \chi_1}{\partial \kappa_2} & \frac{\partial \chi_1}{\partial \chi_2} \end{bmatrix} \right) \right| = \left| 1 + \kappa_2 \frac{\partial s_0}{\partial \lambda_2} + \chi_2 \frac{\partial s_0}{\partial \kappa_2} \right| \quad (25)$$

From Eq. (23) we find that

$$\frac{\partial s_0}{\partial \lambda_2} = -\frac{6}{3\kappa_2 + 2\chi_2 s_0} \quad (26)$$

$$\frac{\partial s_0}{\partial \kappa_2} = -\frac{3s_0}{3\kappa_2 + 2\chi_2 s_0} \quad (27)$$

And thus:

$$\left| \det \left(\frac{d\lambda_1 d\kappa_1 d\chi_1}{d\lambda_2 d\kappa_2 d\chi_2} \right) \right| = \left| \frac{-3\kappa_2 - \chi_2 s_0}{3\kappa_2 + 2\chi_2 s_0} \right| = \left| \frac{6\lambda_2}{3\kappa_2 s_0 + 2\chi_2 s_0^2} \right| \quad (28)$$

If the excited state of the double-well potential is close to the spinodal case, λ_2 is small (as it is in Fig. 12). In particular, when $\lambda_2 \approx 0$, it follows that $s_0 \approx -3\kappa_2/\chi_2$. Inserting this in Eq. (28) gives:

$$\left| \det \left(\frac{d\lambda_1 d\kappa_1 d\chi_1}{d\lambda_2 d\kappa_2 d\chi_2} \right) \right| \simeq \frac{2\lambda_2 \chi_2}{3\kappa_2^2} \simeq \frac{\lambda_2}{\lambda_1} \sim \lambda_2 \quad (29)$$

where λ_1 is a large value with the lower bound ω_c^2 . We have thus found that the joint distribution

$$P(\lambda_2, \kappa_2, \chi_2) \sim \lambda_2 P(\lambda_1, \kappa_1, \chi_1) \quad (30)$$

Hence, the marginal distribution $P(\lambda_2) \sim \lambda_2$ (after integrating out κ_2 and χ_2) and therefore

$$D(\omega_2) = P(\lambda_2) \frac{d\lambda_2}{d\omega_2} \sim \omega_2^3. \quad (31)$$

Gap in energy barrier distribution

For a given λ_1 we define $c(\kappa_1, \chi_1) = \lambda_1 \chi_1 / \kappa_1^2$, which smoothly varies in a narrow range from 1/3 (for a symmetric double-well) to 3/8 (for a spinodal). Then we can express the energy barrier as

$$\Delta E = \lambda_1^2 \frac{(3 - \sqrt{9 - 24c})^2 (-3 + 12c + \sqrt{9 - 24c})}{192 \chi_1 c^2} \quad (32)$$

The function c is slowly varying and not singular so that

$$\Delta E \sim \lambda_1^2 \sim \omega_c^4 \quad (33)$$

Similarly, the energy difference

$$E_{12} = \lambda_1^2 \frac{(3 + \sqrt{9 - 24c})^2 (-3 + 12c - \sqrt{9 - 24c})}{192 \chi_1 c^2} \sim \lambda_1^2 \sim \omega_c^4 \quad (34)$$

(except in the case of a symmetric double-well).

F Estimation of χ_1

Numerically, the coefficient χ_1 (from Eq. (2)) along the direction of the displacement field \vec{s} from the initial minimum to the new minimum whose frequency is smaller than ω_e (the frequency of first tranverse plane waves), can be expressed by the pair interaction $\varphi(\vec{r})$ at mechanical equilibrium, as follows:

$$\chi_1 = \sum_{\alpha, \beta, \eta, \nu=1}^3 \sum_{n, m, k, l=1}^N \frac{\partial^4 U}{\partial r_n^\nu \partial r_m^\eta \partial r_k^\beta \partial r_l^\alpha} s_l^\alpha s_k^\beta s_m^\eta s_n^\nu \quad (35)$$

$$= \sum_{i < j} \left\{ \left(\frac{1}{r_{ij}^4} \frac{d^4 \varphi}{dr^4} - \frac{6}{r_{ij}^5} \frac{d^3 \varphi}{dr^3} + \frac{15}{r_{ij}^6} \frac{d^2 \varphi}{dr^2} - \frac{15}{r_{ij}^7} \varphi' \right) (\vec{r}_{ij} \cdot \vec{s}_{ij})^4 \right. \quad (36)$$

$$\left. + \left(\frac{1}{r_{ij}^3} \frac{d^3 \varphi}{dr^3} - \frac{3}{r_{ij}^4} \frac{d^2 \varphi}{dr^2} + \frac{3}{r_{ij}^5} \varphi' \right) 6 (\vec{r}_{ij} \cdot \vec{s}_{ij})^2 (\vec{s}_{ij} \cdot \vec{s}_{ij}) + \left(\frac{1}{r_{ij}^2} \frac{d^2 \varphi}{dr^2} - \frac{1}{r_{ij}^3} \varphi' \right) 3 (\vec{s}_{ij} \cdot \vec{s}_{ij})^2 \right\} \quad (37)$$

where \vec{r}_i are the particles' equilibrium positions, \vec{s} is the direction (the normalised displacement field from the quenched states before and after reheating), and $\vec{s}_{ij} = \vec{s}_i - \vec{s}_j$.

From the results in Fig. 13 we observe that at small λ_1 , χ_1 is independent of λ_1 . Hence, we regard it as a constant. Here we estimate $\chi_1 \approx 1500$ by its median value. Note that χ_1 has unit $m\omega_0^2/d_0^2$, where m is the particle mass, d_0 is approximately equal to the inter-particle distance a (hence we take $a = d_0$), and $\omega_0 \equiv 1/t_0$ is the unit frequency in our simulation which is about $\omega_D/18$. Here ω_D is the Debye frequency. Hence we get $\chi_1 \approx 1500m\omega_0^2/a^2 \approx 4.6m\omega_D^2/a^2$.

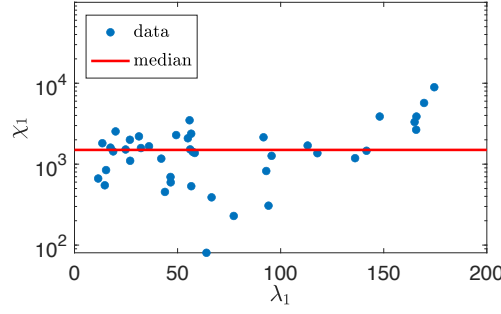


Figure 13. Scatter plot χ_1 as function of λ_1 for our largest gap ($\omega_c = 1.64$). λ_1 follows as $\lambda_1 = \sum_{\alpha,\beta=1}^3 \sum_{k,l=1}^N s_l^\alpha H_{lk}^{\alpha\beta} s_k^\beta$.

The relation between ω_D and ω_0 is calculated by: $\omega_D = (9N/(4\pi(2\omega_e^{-3} + \omega_l^{-3})))^{1/3} \approx 18\omega_0$, where $\omega_e = 1.26\omega_0$ and $\omega_l \approx 2.5\omega_e$ (ω_l is the frequency of first longitudinal modes). Note that both are plane waves. In particular, the first transverse modes consist of 12 modes and the first longitudinal modes consist 6 modes. Their identification is straightforward through the number of modes and their participation ratios, which are around 0.6. Note that $\omega_0 = 1$ in our simulation, so $\omega_D \approx 18$ and $\omega_c/\omega_D \approx 0.1$.

G Geometry of rearrangements

Protocol to separate rearrangements

The displacement field between the states before and after reheating may contain more than one elementary excitation. We extract them one-by-one from this displacement field, by assuming them linearly independent. This corresponds to the following algorithm:

1. Find the particle with the largest displacement.
2. Place a small sphere centred at this particle with a radius $\tilde{R}^{(i)} = (V/N)^{1/3}$ (with i the increment number, starting at $i = 0$).
3. Set all displacements outside the sphere equal to zero. The particle displacements inside the sphere are not changed.
4. Minimise the energy U (every particle is free to move).
5. Increase the radius of sphere: $\tilde{R}^{(i+1)} = \tilde{R}^{(i)} + \Delta\tilde{R}$, and reset the displacements as in step 3 (the particle displacements outside the sphere are set to zero and those inside the sphere equal to the original particle displacements).
6. Repeat steps 4 and 5, until the localised mode is identified. In particular, stop when $|U^{(i+1)} - U^{(i)}| < 10^{-6}$ and, to avoid stopping too early, the norm of the displacement field is larger than 10^{-2} . Note that $U^{(i)}$ refers to the potential energy after energy minimisation, in step 4, for increment i .

The local rearrangement is then the displacement field after the last energy minimisation. We then subtract it from the original displacement and continue to extract the next elementary excitation, by repeating this algorithm. We continue to do so until we have extracted all elementary excitations. In particular, we stop $\tilde{R}^{(i)}/L > \sqrt{3}/2$ (with L the linear size of the simulation box).

Results

Five representative samples (for two different K) showing our separation protocol are shown in Fig. 14, whereby the displacement field of each elementary excitation is plotted using a different colour. On average,

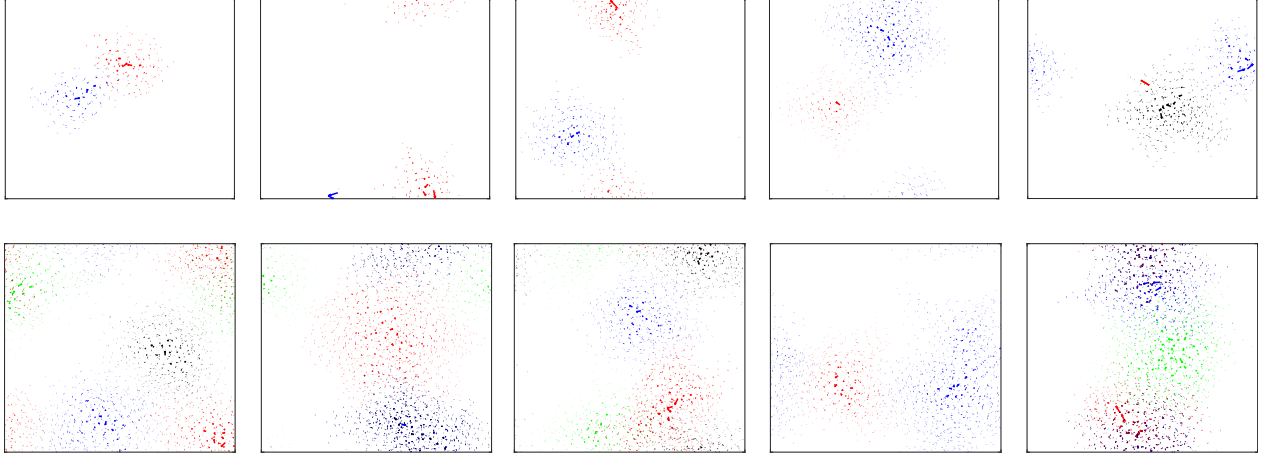


Figure 14. Individual local rearrangements projected on the xy plane, shown using different colours, in five randomly chosen examples (from those samples that show more than one local rearrangement) for: (top) $K = 10^2$, $T_a = 0.15$, and $t_a = 500$, (bottom) $K = 10^4$, $T_a = 0.03$, and $t_a = 500$.

we measure $\{1.4, 1.6, 1.9, 3.5\}$ elementary excitations for $K = \{10^2, 10^3, 3 \times 10^3, 10^4\}$ at the lowest thermal activation $T_a = \{0.15, 0.07, 0.03, 0.03\}$ with $t_a = 500$.

We, furthermore, include the distribution of the participation ratio of the elementary excitations in Fig. 15(a), whereby the different colours correspond to the different data points in Fig. 5(a). We observe that the elementary excitations become more localised for larger gaps. Likewise, we include the distribution of the maximum displacement of each elementary excitation in Fig. 15(b) (the different colours correspond to the different data points in Fig. 5(b)). In this case we observe that the maximum displacement increases for our largest ω_c (in black) as the result of string-like motion. This is supported by the distinct part of the Van Hove correlation in Fig. 15(c) that displays a sharp peak around $r = 0$ only for our largest ω_c (in black). For this configuration, we plot the distribution of the number of permuting particles, $\#n_p$, inside the ‘string’ in Fig. 15(d).

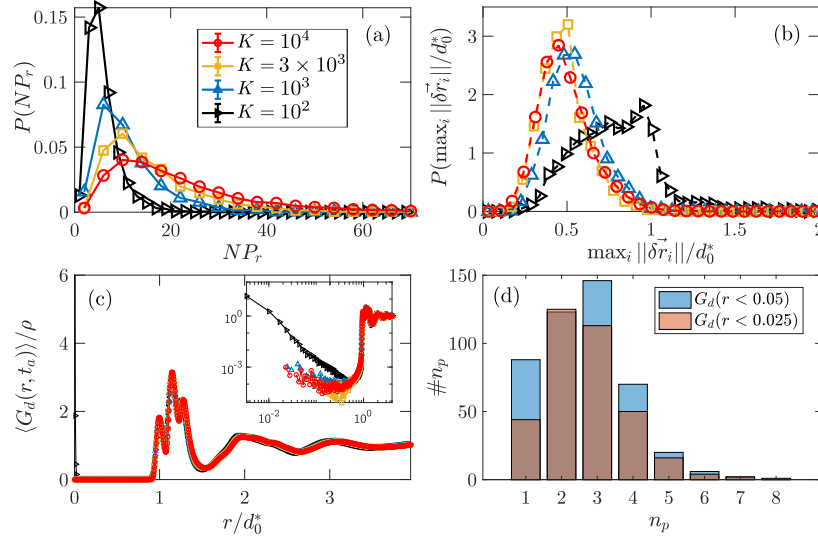


Figure 15. Probability distribution of (a) the participation ratio NP_r and (b) the maximal particle displacement $\max_i\{\|\delta\vec{r}_i\|\}$ at different ω_c . (c) The distinct part of the Van Hove correlation normalised by the number density $\langle G_d \rangle / \rho$ at different ω_c . (d) Histogram of the number of particles that permute per realisation, $\#n_p$ (for largest ω_c) at two different cutoff distances $r_c/d_0^* = \{0.025, 0.05\}$.